Polymer Chemistry

ROYAL SOCIETY OF CHEMISTRY

PAPER

View Article Online
View Journal

Cite this: DOI: 10.1039/d6py00109b

Linkage effects of phenanthrene-based polymeric anodes for lithium-ion batteries

Yu-Ruei Kung, *[a,b] Huai-Sheng Chin,[b] Santosh U. Sharma, [c] Li Chen,[c] Zi-Yun Ou[c] and Hung-Ju Yen *[c]

Organic polymer anodes are increasingly recognized as promising alternatives to graphite due to their structural tunability, surface-dominated lithium-ion storage, and intrinsic safety advantages. However, establishing clear molecular design principles that connect polymer structure to lithium-storage kinetics and electrochemical performance remains a major challenge. In particular, the role of linkage chemistry in regulating lithium-ion storage behavior is often oversimplified and poorly understood. Herein, a systematic series of polyamides (**PQ-polyamide**) featuring identical aryloxy-phenanthrene backbones but distinct linkages is designed to elucidate the influence of the linker on lithium-ion storage behavior. By isolating linkage effects while maintaining a constant redox-active backbone, we demonstrate that substituent engineering plays a decisive role in determining reversible capacity, rate capability, and charge-storage kinetics. Electrochemical analyses reveal that all polymers store lithium predominantly through surface-controlled processes, while the extent of pseudocapacitive contribution varies significantly with linkers. Among the series, **PQ-d** incorporating a diphenyl ether linker delivers the highest reversible capacity of 470 mAh g^{-1} after 100 cycles at 0.1 A g^{-1} and exhibits the largest surface-controlled contribution, as evidenced by *b* values approaching unity and dominant capacitive behavior. A comparative kinetic analysis indicates that linkages promoting conformational flexibility and balanced electronic character facilitate enhanced accessibility of redox-active sites and rapid lithium-ion storage. In contrast, excessively rigid or strongly electron-withdrawing substituents lead to diffusion limitations and reduced electrochemical utilization. This work establishes substituent engineering as an effective molecular strategy for regulating lithium-ion storage kinetics in polyamide-based anodes and provides general design guidelines for the development of organic electrode materials.

Received 1st February 2026,
Accepted 26th April 2026

DOI: 10.1039/d6py00109b

rsc.li/polymers

Introduction

The rapid expansion of electric vehicles, portable electronics, and grid-scale energy storage systems has driven an urgent demand for lithium-ion batteries with higher energy density, faster charge–discharge capability, and improved safety.[1–3] Currently, graphite dominates the commercial anode market owing to its low cost, mature manufacturing infrastructure, and stable cycling performance.[4] Nevertheless, graphite suffers from inherent limitations associated with its intercalation-based lithium-storage mechanism.[5] At high current densities, sluggish solid-state lithium diffusion leads to severe polarization, rapid capacity decay, and non-uniform lithium deposition.[6–8] These issues not only limit rate performance but also raise safety concerns related to lithium plating and dendrite formation during fast charging.[9–12]

To overcome these limitations, alternative anode materials based on fundamentally different lithium-storage mechanisms have been actively explored.[13,14] Among them, organic polymer electrodes have emerged as particularly attractive candidates.[15,16] Unlike inorganic intercalation hosts, polymers store lithium ions mainly through localized redox reactions involving π-conjugated frameworks and heteroatom-containing functional groups.[17,18] Such surface or near-surface redox processes significantly reduce dependence on long-range lithium diffusion, enabling rapid charge–discharge kinetics and more homogeneous lithium-ion flux.[19,20] Consequently, polymer anodes are expected to suppress lithium dendrite formation and improve operational safety, especially under high-rate conditions. Another key advantage of polymer electrodes lies in their molecular-level tunability.[21] Through rational chemical design,[22] polymer backbones[23] and side-chain substituents can be precisely tailored to modulate electronic structure,

[a]Department of Chemical Engineering and Biotechnology, National Taipei University of Technology, Taipei 10608, Taiwan. E-mail: yrkung@ntut.edu.tw
[b]Department of Chemical Engineering and Biotechnology, Tatung University, Taipei 10452, Taiwan
[c]Institute of Chemistry, Academia Sinica, Taipei 11529, Taiwan. E-mail: hjyen@gate.sinica.edu.tw

redox potential, mechanical flexibility, and ion-electron transport properties.[21,24] This structural versatility offers a powerful platform for establishing structure–property relationships that are difficult to achieve in conventional inorganic materials.[25,26] However, despite these advantages, the development of high-performance polymer anodes remains largely empirical, and clear molecular design principles are still lacking.[22,27]

Polyamides represent a particularly promising class of polymer electrode materials. Their chemically robust backbones, rich heteroatom content, and strong intermolecular interactions endow them with good structural stability and multiple lithium-ion interaction sites.[28–30] Previous studies have shown that lithium ions can interact not only with aromatic π systems but also with amide nitrogen and carbonyl oxygen atoms, enabling multi-site lithium coordination within the polymer framework.[31,32] Moreover, polyamide backbones can be readily functionalized through side-chain modification, providing an ideal platform for systematic structural tuning.[33]

Several studies have explored structure–property relationships in polymer electrode materials, focusing on factors such as backbone conjugation, heteroatom incorporation, and substituent electronic effects.[15,34] For instance, conjugated polymers and polyimide-based electrodes have shown that increased π-conjugation and electron-withdrawing groups can enhance electronic conductivity and redox reversibility.[35,36] However, in most reported systems multiple structural parameters are modified simultaneously, making it difficult to isolate the intrinsic influence of linkage chemistry on lithium-ion storage behavior. Further these studies have highlighted the potential of organic electrode materials for rechargeable batteries, where carbonyl- and quinone-based compounds typically deliver reversible capacities of ~150–300 mAh g^{-1} depending on the number of redox-active sites and molecular structure.[37–39] In addition, the structural tunability, low cost, and environmental compatibility of organic materials make them promising candidates for next-generation metal-ion batteries (Scheme 1).[29,40]

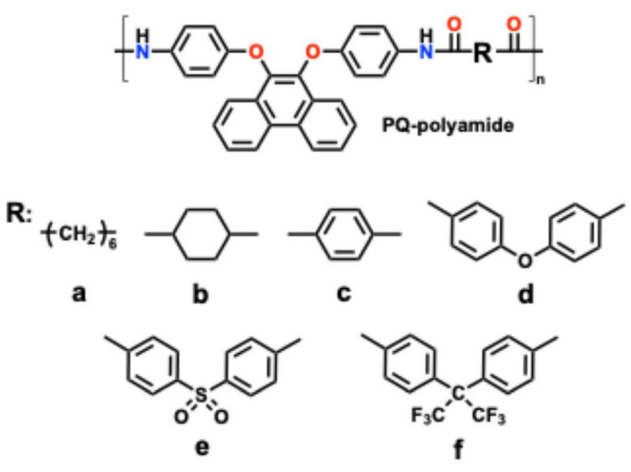

Scheme 1 Chemical structures of **PQ-polyamides**.

Despite these advantages, most existing polyamide-based electrode studies focus on improving performance through backbone modification or increasing redox-active unit density, while the influence of substituent chemistry is often treated as a secondary factor.[41] In many cases, linkage effects are discussed solely in terms of electron-donating or electron-withdrawing strength.[42,43] Such an oversimplified electronic perspective neglects other critical factors, including steric hindrance, conformational flexibility, backbone planarity, and accessibility of redox-active sites.[44,45] These structural and kinetic factors can play an equally important role in determining lithium-ion storage behavior, particularly for surface-dominated polymer electrodes.[46,47] In reality, extended aromatic linkers may increase the density of accessible π systems for lithium–π interactions, while flexible linkages can enhance electrolyte penetration and expose buried redox sites. Conversely, rigid or strongly electron-withdrawing substituents may stabilize electronic states but hinder ion transport or reduce redox kinetics. Disentangling these effects requires a carefully controlled molecular system in which the polymer backbone remains constant while the linkage structure is systematically varied.[48–50] To address this challenge, we design and synthesize a series of polyamides denoted as **PQ-polyamides**. Although structure–property correlations in polymer electrodes have been widely investigated, most studies involve simultaneous variations in backbone structure, redox-active units, or conjugation length, making it difficult to isolate the intrinsic role of linkage chemistry.[51] In contrast, the present study adopts a controlled molecular design in which all polymers share an identical aryloxy-phenanthrene redox-active backbone while only the linkage structure is systematically varied. This strategy allows the influence of linkage chemistry on lithium-ion storage behavior to be examined independently from backbone-related effects. Beyond conventional electronic considerations, the results reveal that linkage chemistry can regulate lithium-storage kinetics through multiple structural factors, including conformational flexibility, accessibility of redox-active sites, and interfacial lithium-ion transport. By establishing a direct correlation between linkage structure and electrochemical kinetics, this work provides new molecular-level insights into polymer electrode design that extend beyond previously reported studies focusing primarily on backbone modification or substituent electronics.

In addition to backbone conjugation and heteroatom density, linkage chemistry represents an important yet underexplored molecular design parameter in polymer electrodes. While backbone modification directly alters the intrinsic redox framework and heteroatom density determines the number of potential coordination sites for lithium ions, linkage structures can influence electrochemical behavior through multiple structural and kinetic factors. These include conformational flexibility of the polymer chain, steric accessibility of redox-active sites, intermolecular packing, and electrolyte penetration within the polymer matrix. Because linkage modification can regulate these properties without altering the fundamental redox-active backbone, it offers a versatile strategy

for tuning lithium-ion storage kinetics while preserving the intrinsic electrochemical functionality of the polymer framework. Therefore, systematic investigation of linkage chemistry provides a complementary and potentially generalizable design lever for optimizing polymer-based electrode materials.

To implement this design strategy, we synthesized a series of polyamides denoted as **PQ-polyamides**, all sharing an identical aryloxy-phenanthrene backbone but incorporating six distinct linkers with different aromaticity, linkage chemistry, and electronic characteristics. This molecular platform enables direct comparison of linkage effects on lithium-ion storage behavior without interference from backbone variations. Through systematic electrochemical characterization, including galvanostatic cycling, rate capability testing, and cyclic voltammetry (CV) based kinetic analyses, we establish clear correlations between linkage structure and electrochemical performance. The results demonstrate that linkages balancing π-conjugation, conformational flexibility, and electronic neutrality promote dominant surface-controlled lithium storage and improved rate capability. These findings provide mechanistic insights into linkage-regulated charge-storage kinetics and offer molecular design guidelines for the development of high-performance organic polymer electrodes.

Results and discussion

Structural considerations and scope of this study

The molecular structures, synthesis routes, film-forming behavior, thermal stability, solubility, and detailed physicochemical characterizations of the **PQ-polyamides** series have been comprehensively reported in our previous work.[52] Briefly, all polymers share an identical aryloxy-phenanthrene polyamide backbone and differ only in the linkage introduced *via* dicarboxylic acid skeletons. These polymers exhibit high molecular weight, amorphous morphology, excellent thermal stability, and good processability, ensuring that differences observed in electrochemical behavior arise primarily from the incorporated linkers. In the present work, we therefore focus exclusively on elucidating how systematic linkage variation influences lithium-ion storage behavior, electrochemical performance, and charge-storage kinetics in these phenanthrene-based polyamide anodes.

Compared with previously reported organic polymer electrodes, where electrochemical performance is typically tuned through modification of the redox-active backbone or by increasing the density of redox sites, the present study adopts a different molecular design strategy. Most prior studies introduce new functional groups or extend conjugation along the polymer backbone, making it difficult to decouple backbone effects from substituent contributions. In contrast, the **PQ-polyamide** system used here maintains an identical aryloxy-phenanthrene backbone while systematically varying only the linkage structure. This controlled molecular framework enables direct evaluation of how linkage chemistry influences lithium-ion storage behavior, charge-storage kinetics, and electrochemical accessibility of redox-active sites, thereby providing clearer mechanistic insight into substituent-driven kinetic regulation in polymer electrodes. The key physicochemical parameters of the polyamides, including inherent viscosity, glass transition temperature, and thermal stability, are summarized in Table S1 for clarity.

Electrochemical redox behaviour of PQ-polyamides

To elucidate the lithium-ion storage behavior of **PQ-polyamides** series, the electrochemical properties were systematically investigated using half-cell configurations with lithium metal as the counter and reference electrode (SI note S1). As all polymers share an identical aryloxy-phenanthrene backbone and differ only in their linkages, this system provides an ideal platform to evaluate linkage-driven effects on electrochemical performance. By combining CV, galvanostatic charge–discharge (GCD) measurements, and kinetic analyses, we aim to establish clear correlations between linkage, lithium-ion storage mechanism, and electrochemical properties. The following discussion focuses on how variations in linkage chemistry influence redox behavior, specific capacity, rate capability, and charge-storage kinetics, while the fundamental lithium-storage mechanism remains governed by the polyamide backbone.

Fig. 1 shows the cyclic voltammograms of **PQ-polyamides** recorded for a representative single cycle in the voltage range of 0.02–3.0 V (*vs.* Li/Li^+) at a scan rate of 0.1 mV s^{-1} (see Fig. S1 for full cycles). All polymers exhibit similar overall CV profiles, indicating that lithium-ion storage is predominantly governed by the identical aryloxy-phenanthrene polyamide backbone. During the cathodic sweep, a pronounced reduction feature appears at very low potential (~0.02 V) for all samples, which can be attributed to deep lithiation of the conjugated aromatic framework through Li^+–π interactions involving the aromatic phenanthrene backbone and linkages. A broader reduction peak located at intermediate potentials (~0.76–0.86 V) is associated with lithium-ion coordination at heteroatom-containing sites, such as amide nitrogen and carbonyl oxygen atoms. In the anodic sweep, a broad oxidation peak centered at ~0.93–0.96 V corresponds to the reversible extraction of lithium ions from the lithiated polymer matrix, while a weaker oxidation shoulder at higher potentials (~2.44–2.47 V) is related to the delithiation of more weakly bound or surface-accessible lithium species, indicating a largely reversible redox process.[53–55] Although the fundamental redox mechanism remains similar across the series, the magnitude of the current response varies significantly depending on the linkage. Polymers bearing aromatic linkers (**PQ-c** to **PQ-f**) exhibit higher current densities than that of aliphatic analogues (**PQ-a** and **PQ-b**), reflecting an enhanced lithium-ion storage activity arising from additional π-conjugated systems.

Although all polymers exhibit broadly similar CV profiles, the differences in current response are relatively subtle in the representative single-cycle curves and should therefore be interpreted with caution. Rather than relying on visual comparison of a single CV trace, the electrochemical ranking dis-

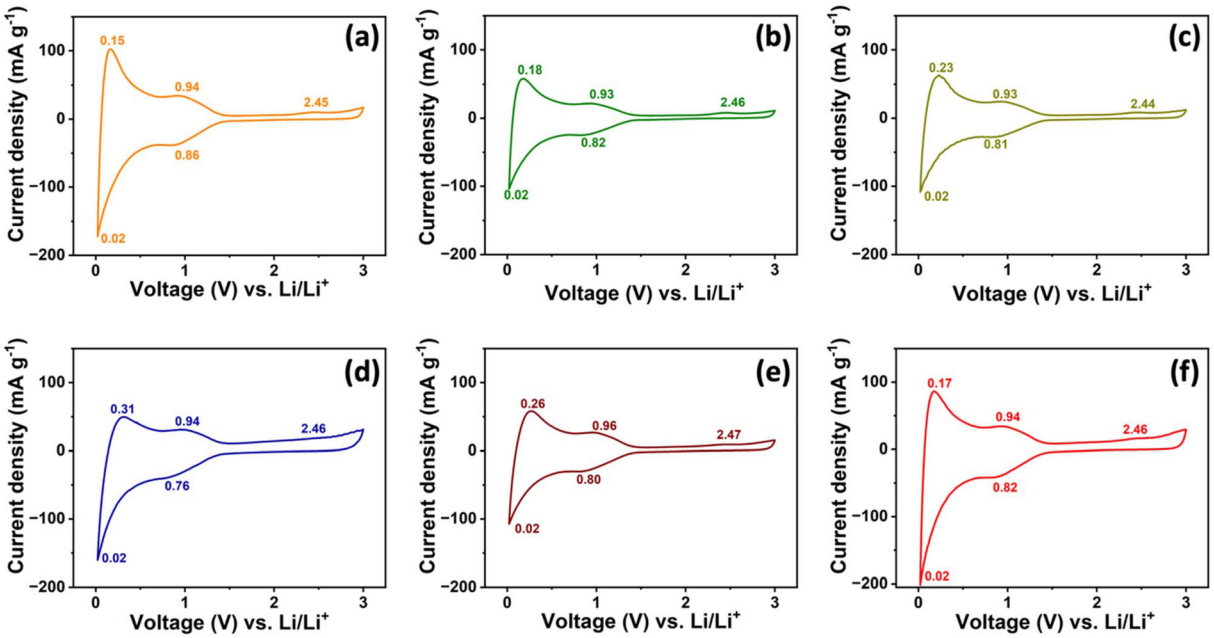

Fig. 1 Cyclic voltammograms of (a) **PQ-a**, (b) **PQ-b**, (c) **PQ-c**, (d) **PQ-d**, (e) **PQ-e**, and (f) **PQ-f** recorded for a representative single cycle in the voltage window of 0.02–3.0 V (*vs.* Li/Li$^+$) at a scan rate of 0.1 mV s^{-1}.

cussed here is based on the combined trends from cyclic voltammetry at multiple scan rates (Fig. S2), galvanostatic charge–discharge capacities, and rate-performance measurements. In this context, **PQ-c** and **PQ-d** exhibit comparatively stronger electrochemical utilization, whereas **PQ-e** and **PQ-f** show lower reversible capacities and weaker overall electrochemical response. These results demonstrate that while the polyamide backbone determines the intrinsic lithium-storage mechanism, linkage plays a critical role in regulating lithium-ion accessibility and electrochemical activity, which is further reflected in the subsequent cycling and kinetic analyses.

Following the redox features observed in CV, the lithium-ion storage capability of **PQ-polyamides** was further evaluated by GCD measurements at a current density of 0.1 A g^{-1} (≈0.06 C) within a voltage window of 0.02–3.0 V (*vs.* Li/Li$^+$), as shown in Fig. 2. All polymers exhibit a pronounced irreversible capacity loss during the first cycle, which is characteristic of organic electrode materials and can be attributed to electrolyte decomposition and solid-electrolyte interphase (SEI) formation, particularly at low potentials where deep lithiation of the conjugated framework occurs.[56] Notably, **PQ-d** exhibits the highest initial discharge capacity among the series, exceeding ~600 mAh g^{-1} at the first cycle, indicating extensive lithium uptake during the initial lithiation process.

After the initial activation, charge–discharge profiles gradually stabilize upon subsequent cycling, reflecting the establishment of a more reversible lithiation–delithiation process, in agreement with the largely reversible redox behavior observed in the CV curves. Clear differences in reversible capacity are observed among the six polymers despite the presence of the same aryloxy-phenanthrene redox-active unit in their polymer chains. These differences likely arise from variations in the linker structures, which can influence polymer chain packing, free volume, and accessibility of the redox-active sites. For example, the diphenyl ether linkage present in **PQ-d** introduces an angled yet relatively rigid structural motif that may increase chain spacing and free volume, potentially facilitating electrolyte penetration and lithium-ion access to the polymer matrix. Upon prolonged cycling, **PQ-d** maintains the highest reversible capacity, stabilizing at approximately 470 mAh g^{-1} after 100 cycles, followed by **PQ-c** with a capacity of around 290 mAh g^{-1}. **PQ-a**, **PQ-b**, and **PQ-e** exhibit moderate capacities in the range of 190–220 mAh g^{-1}, while **PQ-f** delivers the lowest capacity, remaining below 160 mAh g^{-1}. The gradual capacity increase observed during the early cycles for most samples can be attributed to progressive activation of redox-active sites and improved electrolyte penetration into the polymer matrix.[57–59] The overall capacity trend closely follows the CV current responses discussed earlier. Polymers showing higher current densities in the CV measurements, particularly **PQ-d** and **PQ-c**, also exhibit higher initial and reversible capacities under galvanostatic conditions, suggesting more effective utilization of redox-active sites. In contrast, **PQ-f** displays limited capacity, consistent with kinetically hindered lithium-ion storage. These results confirm that while the polyamide backbone governs the intrinsic lithium-storage mechanism, the linkage structure critically determines the extent of lithium uptake and its reversibility during cycling.

Building on the linkage-dependent redox response observed in the CV curves and the distinct reversible capacities seen in the GCD profiles, we next evaluated the long-term cycling stability and rate performance of **PQ-polyamides** to clarify how

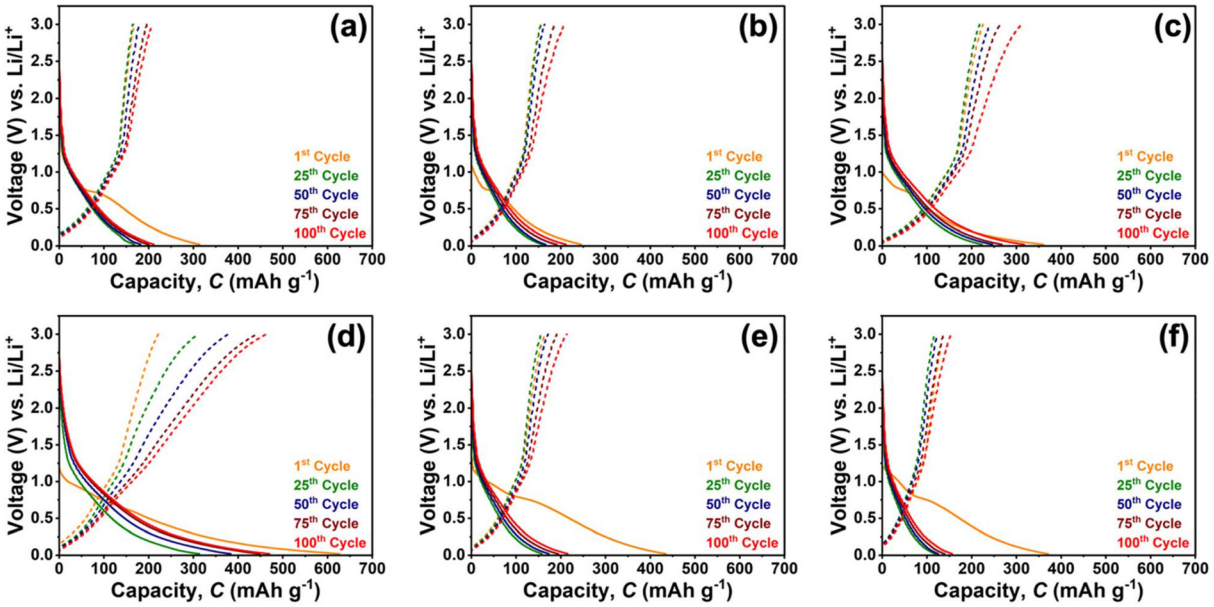

Fig. 2 Galvanostatic charge–discharge profiles of (a) **PQ-a**, (b) **PQ-b**, (c) **PQ-c**, (d) **PQ-d**, (e) **PQ-e**, and (f) **PQ-f** measured at 0.1 A g^{-1} within a voltage range of 0.02–3.0 V (*vs.* Li/Li^+).

linkage chemistry controls practical lithium-storage behavior. As shown in Fig. 3a, all electrodes exhibit stable cycling at 0.1 A g^{-1} (≈0.06 C), with coulombic efficiencies stabilize near unity after the initial activation stage, indicating that the lithiation–delithiation process becomes highly reversible once the SEI and electrode/electrolyte interface are stabilized. The gradual increase in reversible capacity observed during the first several cycles is attributed to electrode activation and improved electrolyte wetting within the polymer matrix. Consequently, the coulombic efficiency values during the early cycles should be interpreted with caution, as small fluctuations may occur before the electrochemical system stabilizes. Notably, **PQ-d** shows the most pronounced capacity activation and delivers the best overall cycling performance, increasing

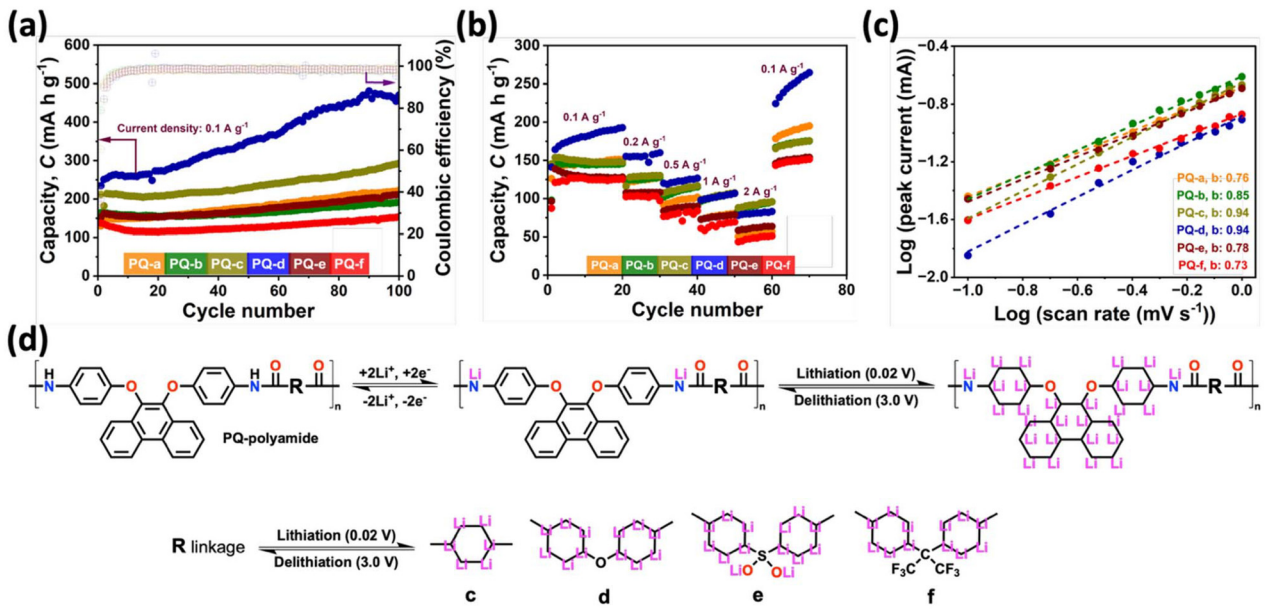

Fig. 3 (a) Cycling performance measured at a current density of 0.1 A g^{-1}; (b) rate capability evaluated at different current densities ranging from 0.1 to 2.0 A g^{-1}; (c) *b*-value determination based on the relationship between peak current and scan rate; and (d) schematic illustration of the lithium-ion storage mechanism in **PQ-polyamides**, highlighting Li^+ coordination with heteroatoms and Li^+–π interactions within the conjugated backbone and substituent-derived aromatic systems.

steadily to ~470 mAh g^{-1} after 100 cycles, consistent with its stronger current response in CV and its higher lithium utilization under galvanostatic cycling. **PQ-c** maintains the second-highest capacity (≈290 mAh g^{-1}), whereas **PQ-a**, **PQ-b**, and **PQ-e** exhibit moderate capacities (≈190–220 mAh g^{-1}). In contrast, **PQ-f** remains the lowest-performing electrode (≲160 mAh g^{-1}), suggesting that lithium uptake is kinetically restricted and/or less reversible despite the presence of aromatic content. The overall trend confirms the conclusion drawn from the CV and GCD results: while the polyamide backbone governs the remembering redox motif, the linkage strongly dictates the fraction of redox sites that are electrochemically accessible over repeated cycling. Rate capability measurements further highlight the substituent-controlled kinetic differences (Fig. 3b). With increasing current density from 0.1 to 2.0 A g^{-1}, all polyamide electrodes show the expected decrease in capacity due to increased polarization; however, **PQ-d** consistently delivers the highest capacity at low-to-moderate rates and shows good recovery when the current is returned to 0.1 A g^{-1}, demonstrating robust structural reversibility and stable interfacial behavior. Interestingly, at the highest current density of 2.0 A g^{-1}, **PQ-c** becomes comparable to or slightly better than **PQ-d**, implying that although **PQ-d** enables higher utilization at low rates, **PQ-c** may possess marginally faster charge–discharge response under an extreme polarization. Table S2 summarizes the various type of polymer-based anodes used for LIBs. To quantitatively probe the charge-storage mechanism behind these trends, the relationship between peak current and scan rate was analyzed (Fig. 3c). The corresponding CV curves at various scan rates are shown in Fig. S2. The derived *b* values follow the order **PQ-c** (0.94) ≈ **PQ-d** (0.94) > **PQ-b** (0.85) > **PQ-e** (0.78) > **PQ-a** (0.76) > **PQ-f** (0.73), indicating that **PQ-c** and **PQ-d** exhibit a larger capacitive contribution, suggesting faster surface-controlled charge storage kinetics than others. This kinetic hierarchy explains why **PQ-c** and **PQ-d** maintain superior capacity retention at higher rates and why **PQ-f** performs poorly overall.

Li^+ storage mechanism studies

During the lithiation process, lithium ions are inserted into the polyamide framework accompanied by a reduction of the π-conjugated structure, while delithiation involves the extraction of lithium ions and the recovery of the polymer backbone to its original electronic state. By varying only, the chemical structure of the linkages, the possible lithium-ion interaction sites and the maximum lithiation scenarios were proposed for mechanistic discussion, as schematically illustrated in Fig. 3d.

From the perspective of the polymer backbone, previous studies on lithium-aromatic interactions have suggested that a benzene ring can theoretically accommodate up to six lithium ions under an idealized and highly lithiated state.[60] In addition to aromatic π systems, heteroatoms are also expected to participate in lithium-ion coordination. In particular, the nitrogen atoms in amide groups and the carbonyl oxygen atoms can serve as additional lithium-ion interaction sites, thereby facilitating lithium coordination within the polymer framework. Based on the structural features of the aryloxy-phenanthrene polyamide backbone, the maximum lithiation scenario corresponds to the accommodation of up to 30 lithium ions per repeat unit. With respect to the linkages, **PQ-a** and **PQ-b** do not introduce additional conjugated aromatic systems beyond the polymer backbone; consequently, their lithium-ion storage behavior is primarily governed by the phenanthrene backbone. In contrast, **PQ-c** contains an additional benzene ring in the substituent, which introduces an extra aromatic π system from the backbone. Based on lithium-aromatic interaction principles, this additional benzene ring is considered capable of accommodating up to six lithium ions under an idealized lithiation state.[61,62]

For **PQ-d** consisting of two benzene rings linked by an oxygen atom, thereby introducing two additional aromatic π systems, which are theoretically expected to accommodate up to 12 lithium ions in a maximum lithiation scenario. In the case of **PQ-e**, the linkage contains two benzene rings connected through a sulfone group. Considering both the aromatic π systems and the heteroatom-rich sulfone group, **PQ-e** is therefore estimated to accommodate up to 14 lithium ions under maximum lithiation conditions. For **PQ-f** with the linkage also contains two aromatic rings and is accordingly estimated to accommodate a maximum of 12 lithium ions. By summing the contributions from the polymer backbone and linkages, the maximum lithium-ion storage capacities are estimated to be 30 Li^+ for **PQ-a** and **PQ-b**, 36 Li^+ for **PQ-c**, 42 Li^+ for **PQ-d**, 44 Li^+ for **PQ-e**, and 42 Li^+ for **PQ-f** per repeat unit. Based on these values, the theoretical specific capacities were calculated using the equation $C = (n \times F)/3.6$ M (mAh g^{-1}), where C is the theoretical specific capacity, n is the number of electrons participating in the reaction, F is the Faraday constant (96 485 C mol^{-1}) and M is the molecular weight of repeating unit.[53,63,64] Accordingly, the theoretical capacities of **PQ-a**, **PQ-b**, **PQ-c**, **PQ-d**, **PQ-e**, and **PQ-f** are calculated to be 1515, 1444, 1752, 1751, 1707, and 1449 mAh g^{-1}, respectively. It should be noted that this theoretical capacity represents an idealized upper limit based on the assumption that each aromatic ring can accommodate up to six lithium ions through complete reduction of the π-system. In practice, such full lithiation is unlikely to be electrochemically accessible in polymeric electrode materials due to steric constraints, limited electrolyte accessibility, polymer chain packing, and kinetic limitations of lithium-ion transport within the polymer matrix. Therefore, the calculated value should be interpreted only as a theoretical reference point rather than a quantitatively achievable capacity. The experimentally observed capacities are expected to be significantly lower due to these structural and kinetic constraints. It is evident that a substantial gap exists between the theoretically predicted capacities and the experimentally achieved values. This discrepancy is primarily attributed to the difficulty of realizing complete lithiation of all aromatic rings and coordination sites under practical electrochemical conditions. Factors such as kinetic limitations, incomplete accessibility of redox-active sites, steric hindrance, and diffusion constraints restrict the effective utilization of the

theoretical lithium-storage capacity. Consequently, only a fraction of the idealized lithium-ion storage sites participates in reversible electrochemical reactions, resulting in experimentally observed capacities that are significantly lower than the theoretical maxima.

To further quantify the lithium-ion storage mechanism and validate the kinetic trends inferred from the *b*-value analysis, the relative contributions of surface-controlled (capacitive) and diffusion-controlled processes were evaluated using the method proposed by Dunn *et al.*[65,66] According to this approach, the current response at a given potential can be expressed as $i(v) = k_1v + k_2v^{1/2}$, where v is the scan rate, k_1v represents the surface-controlled (capacitive) contribution, and $k_2v^{1/2}$ corresponds to the diffusion-controlled component (SI note S2). By separating these two contributions at different scan rates, the dominant charge-storage mechanism for each polymer electrode can be quantitatively assessed. As shown in Fig. 4, **PQ-polyamide** electrodes exhibit a substantial surface-controlled contribution, which becomes progressively more dominant with increasing scan rate. This behavior indicates that lithium-ion storage in these polyamide electrodes is largely governed by surface or near-surface redox processes rather than long-range solid-state diffusion, consistent with the pseudocapacitive characteristics observed in the CV and *b*-value analyses. The increasing capacitive contribution at higher scan rates further confirms that rapid charge storage is enabled by readily accessible redox-active sites within the polymer framework. Among the six polymers, **PQ-c** and **PQ-d** exhibit the highest capacitive contributions over the entire scan-rate range. Notably, even at a low scan rate of 0.1 mV s^{-1}, **PQ-c** and **PQ-d** already display substantial capacitive contributions of approximately 81.2% and 79.3%, respectively, which are markedly higher than those of other polymers. With increasing scan rate, the capacitive contribution for both electrodes increases further, exceeding 90% at high scan rates. This pronounced surface-controlled behavior is fully consistent with their high *b* values (~0.94) and explains their superior reversible capacity and rate capability observed during galvanostatic cycling.

In contrast, **PQ-f** exhibits a significantly lower capacitive contribution, particularly at low to intermediate scan rates, indicating a comparatively stronger diffusion-controlled component. Although surface-controlled processes still become dominant at high scan rates, the larger diffusion limitation at practical scan rates restricts efficient utilization of redox-active sites, leading to inferior capacity and poorer rate performance. The remaining polymers (**PQ-a**, **PQ-b**, and **PQ-e**) display intermediate behavior, with moderate capacitive contributions that increase gradually with scan rate, reflecting a mixed charge-storage mechanism. Overall, the capacitive-diffusion contribution analysis provides strong quantitative evidence that substituent chemistry directly regulates lithium-ion storage kinetics in **PQ-polyamides**. Linkages that promote extended π-conjugation and conformational flexibility, such as the diphenyl ether group in **PQ-d**, facilitate dominant surface-controlled lithium storage and superior electrochemical performance. These results further corroborate the linkage-kinetics-performance relationship established through CV, rate capability, and *b*-value analyses. It should be noted that *b*-value analysis and Dunn-type capacitive separation provide phenom-

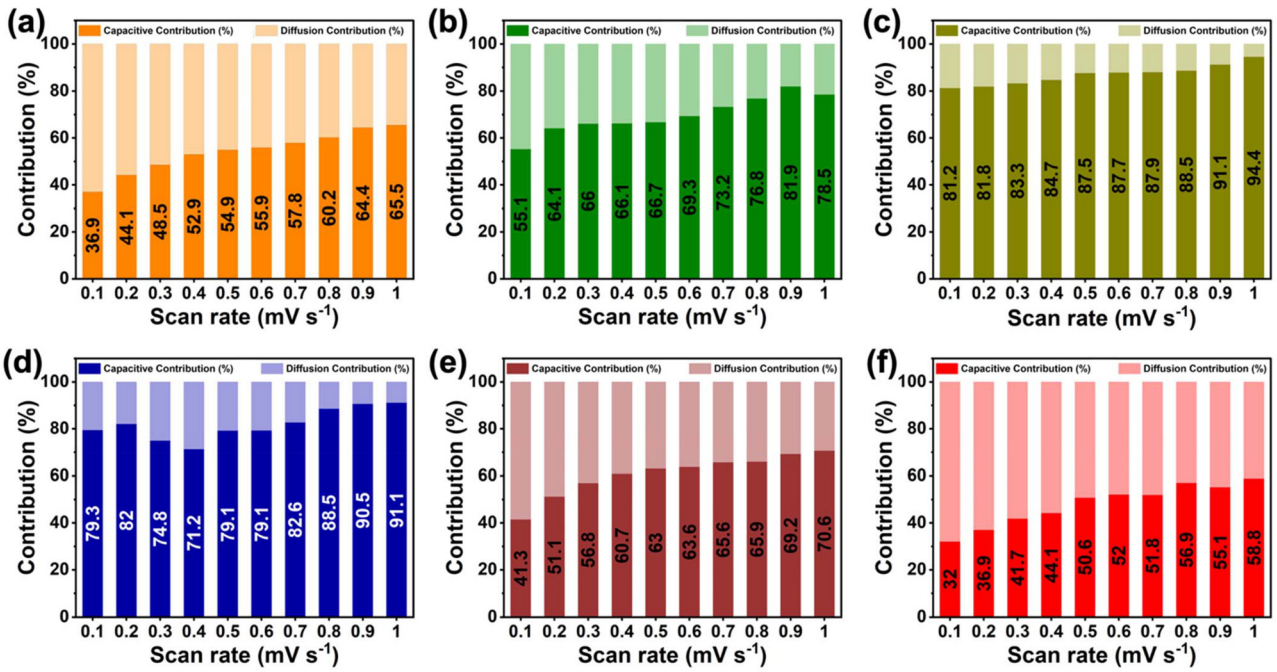

Fig. 4 Quantitative analysis of capacitive and diffusion-controlled charge-storage contributions for **PQ-polyamides** at different scan rates derived using Dunn's method, illustrating the substituent-dependent evolution of surface-controlled lithium-ion storage behavior.

enological insights into charge-storage kinetics and cannot unambiguously distinguish true pseudocapacitive behavior from diffusion-limited processes occurring in porous or disordered electrode structures. Therefore, these analyses are interpreted here as indicators of relative kinetic differences among the polymers rather than definitive mechanistic proof.

In addition, electrochemical impedance spectroscopy (EIS) was conducted to further probe the interfacial charge-transfer characteristics of **PQ-polyamide** electrodes before and after cycling, and the corresponding Nyquist plots are presented in Fig. S3. All electrodes exhibit a depressed semicircle in the high- to medium-frequency region followed by an inclined line at low frequencies, which can be attributed to the combined contributions of charge-transfer resistance at the electrode–electrolyte interface and ion diffusion within the polymer matrix. The absence of a well-defined vertical Warburg region is consistent with the predominantly surface-controlled lithium-ion storage behavior observed from the CV and capacitive contribution analyses.[62]

Upon cycling, noticeable changes in the impedance response are observed for all polymers, reflecting interfacial reconstruction and stabilization of the electrode/electrolyte interface. In general, polymers with higher capacitive contributions and larger *b* values, particularly **PQ-c** and **PQ-d**, exhibit relatively smaller increases in charge-transfer resistance after cycling, indicating more stable interfacial kinetics and efficient lithium-ion transport. In contrast, **PQ-e** and **PQ-f** show significantly larger impedance growth upon cycling, suggesting increased interfacial resistance and slower charge-transfer processes, which is consistent with their lower reversible capacities and rate performance. These EIS results further support the conclusion that substituent chemistry plays a critical role in regulating interfacial charge-transfer behavior in polyamide-based electrodes.

To further elucidate the kinetic characteristics of lithium-ion storage, electrochemical impedance spectra were additionally analyzed in the frequency domain, and the corresponding Bode plots are provided in the SI Fig. S4. In the Bode magnitude plots, **PQ-polyamide** electrodes exhibit a negative slope in the intermediate-frequency region, indicating a gradual transition from kinetically limited interfacial processes at low frequencies to faster electrochemical response at higher frequencies.[67] Such behavior is characteristic of electrodes dominated by surface or near-surface charge-storage processes rather than purely diffusion-controlled lithium transport, consistent with the pseudocapacitive features identified from CV and Dunn analyses[61,62,68] The Bode phase plots reveal a distinct phase-angle minimum for each polymer electrode. The frequency at which this minimum occurs is defined as the knee (characteristic) frequency (*fk*), which reflects the dominant electrochemical relaxation process of the electrode.[68] The associated relaxation time constant (τ) can be estimated according to $\tau = 1/fk$. Based on this analysis, **PQ-a**, **PQ-b**, **PQ-c**, **PQ-d**, **PQ-e**, and **PQ-f** exhibit knee frequencies of approximately 316.24, 343.43, 439.83, 257.33, 235.64, and 637.44 Hz, corresponding to relaxation times of 3.16, 2.91, 2.27, 3.89, 4.24, and 1.57 ms, respectively. Interestingly, **PQ-f** exhibits the shortest relaxation time among the investigated polymers but does not deliver the highest capacity. This observation indicates that fast charge-transfer kinetics alone do not necessarily guarantee high reversible capacity. While a short relaxation time reflects rapid interfacial charge-transfer and ion-transport processes, the achievable capacity also depends on the number and accessibility of electrochemically active sites within the polymer matrix. In the case of **PQ-f**, structural factors such as polymer packing or steric constraints may limit the utilization of redox-active units despite relatively fast kinetic behavior. In general, a higher knee frequency (shorter relaxation time) indicates a faster characteristic electrochemical response to the applied perturbation.[69] Among the series, **PQ-c** and **PQ-d** exhibit relatively short relaxation times while simultaneously delivering high reversible capacities and dominant surface-controlled contributions, indicating an effective balance between rapid interfacial kinetics and accessible redox-active sites. In contrast, **PQ-e** shows the longest relaxation time, reflecting slower electrochemical relaxation and increased kinetic limitations, which is consistent with its lower capacitive contribution and inferior electrochemical performance. Although **PQ-f** displays the shortest relaxation time, its overall lithium-ion storage capability remains limited, suggesting that fast relaxation alone is insufficient to ensure high reversible capacity and that effective utilization and stability of redox-active sites are equally critical.

Conclusion

In this work, we systematically investigated the lithium-ion storage behavior of a structurally well-defined series of polyamides (**PQ-polyamides**) featuring an identical aryloxy-phenanthrene backbone and six distinct linkages. By decoupling backbone redox chemistry from substituent effects, this study provides clear molecular-level insight into how substituent engineering governs electrochemical activity, charge-storage kinetics, and practical battery performance in polymer-based anodes. All polymers exhibit reversible lithium-ion storage dominated by surface-controlled processes; however, pronounced differences in capacity, rate capability, and kinetic response arise solely from variations in substituent structure. Among the series, **PQ-d** delivers the highest reversible capacity and most favourable cycling performance, while **PQ-c** exhibits excellent kinetic response and rate capability. Comprehensive electrochemical analyses including CV, galvanostatic cycling, *b*-value evaluation, capacitive-diffusion contribution analysis, and impedance spectroscopy-collectively demonstrate that substituents promoting extended π-conjugation and conformational flexibility facilitate greater accessibility of redox-active sites and faster interfacial lithium-ion storage. In contrast, rigid or strongly electron-withdrawing substituents impose kinetic limitations, increase interfacial resistance, and restrict effective utilization of theoretical redox sites, leading to inferior electrochemical performance.

Overall, this work establishes substituent engineering as a decisive strategy for regulating lithium-ion storage kinetics and performance in polyamide anodes. Rather than relying solely on increasing redox density or electron-withdrawing strength, optimal battery performance requires a balanced combination of aromatic accessibility, structural flexibility, and interfacial stability. These findings provide generalizable design guidelines for the development of high-performance organic electrode materials and highlight the importance of kinetic and interfacial considerations in advancing polymeric energy storage systems.

Author contributions

Y. R. K. ideated the structures of polymers. H. J. Y. designed the experiments. L. C. performed the electrochemical and characterization experiments. S. U. S. and Z. Y. O. performed the electrochemical data analysis. Y. R. K. and H. S. C. performed the polyamide synthesis and structural characterization. The manuscript was written by S. U. S. and edited by H. J. Y. and Y. R. K. All authors discussed the results and reviewed the manuscript.

Conflicts of interest

There are no conflicts to declare.

Data availability

The data supporting this article have been included as part of the supplementary information (SI). Supplementary information: supplementary notes, cycling voltammetry for full cycles (Fig. S1), cycling voltammetry at various scan rates (Fig. S2), Nyquist plots (Fig. S3), and Bode plots (Fig. S4). See DOI: https://doi.org/10.1039/d6py00109b.

Acknowledgements

The authors acknowledge the funding support from the Ministry of Science and Technology in Taiwan (MOST 111-2221-E-036-001; NSTC 112-2221-E-036-001; NSTC 114-2113-M-001-015; NSTC 114-2113-M-001-018) and Tatung University, Taipei, Taiwan, Republic of China (R.O.C.), grant number B111-C03-008, as well as Innovative Materials and Analysis Technology Exploration in Academia Sinica (AS-iMATE-114-24).

References

1 Z. Zhu, T. Jiang, M. Ali, Y. Meng, Y. Jin, Y. Cui and W. Chen, *Chem. Rev.*, 2022, **122**, 16610–16751.
2 G. G. Njema, R. B. O. Ouma and J. K. Kibet, *J. Renewable Energy*, 2024, **2024**, 2329261.
3 J. Xu, X. Cai, S. Cai, Y. Shao, C. Hu, S. Lu and S. Ding, *Energy Environ. Mater.*, 2023, **6**, e12450.
4 L. Zhao, B. Ding, X. Y. Qin, Z. Wang, W. Lv, Y. B. He, Q. H. Yang and F. Kang, *Adv. Mater.*, 2022, **34**, 2106704.
5 J. Xiao, F. Shi, T. Glossmann, C. Burnett and Z. Liu, *Nat. Energy*, 2023, **8**, 329–339.
6 S. Sarkar and V. Thangadurai, *ACS Energy Lett.*, 2022, **7**, 1492–1527.
7 S. Dong, L. Sheng, L. Wang, J. Liang, H. Zhang, Z. Chen, H. Xu and X. He, *Adv. Funct. Mater.*, 2023, **33**, 2304371.
8 L. Qian, Y. Zheng, T. Or, H. W. Park, R. Gao, M. Park, Q. Ma, D. Luo, A. Yu and Z. Chen, *Small*, 2022, **18**, 2205233.
9 S. Li, K. Wang, G. Zhang, S. Li, Y. Xu, X. Zhang, X. Zhang, S. Zheng, X. Sun and Y. Ma, *Adv. Funct. Mater.*, 2022, **32**, 2200796.
10 W. Huang, Y. Ye, H. Chen, R. A. Vilá, A. Xiang, H. Wang, F. Liu, Z. Yu, J. Xu and Z. Zhang, *Nat. Commun.*, 2022, **13**, 7091.
11 Y. Liu, H. Shi and Z.-S. Wu, *Energy Environ. Sci.*, 2023, **16**, 4834–4871.
12 C.-Y. Wang, T. Liu, X.-G. Yang, S. Ge, N. V. Stanley, E. S. Rountree, Y. Leng and B. D. McCarthy, *Nature*, 2022, **611**, 485–490.
13 Z. Cheng, H. Jiang, X. Zhang, F. Cheng, M. Wu and H. Zhang, *Adv. Funct. Mater.*, 2023, **33**, 2301109.
14 T. Wulandari, D. Fawcett, S. B. Majumder and G. E. Poinern, *Battery Energy*, 2023, **2**, 20230030.
15 F. Baskoro, S. U. Sharma, A. L. Lubis and H.-J. Yen, *J. Mater. Chem. A*, 2025, **13**, 1552–1589.
16 M. Shi and X. Zhang, *Adv. Mater.*, 2025, **37**, 2415676.
17 M. Yin, X. Zhou and Z. Xue, *Macromol. Chem. Phys.*, 2024, **225**, 2300427.
18 S. Haldar, A. Schneemann and S. Kaskel, *J. Am. Chem. Soc.*, 2023, **145**, 13494–13513.
19 M. Cai, Y. Dong, M. Xie, W. Dong, C. Dong, P. Dai, H. Zhang, X. Wang, X. Sun and S. Zhang, *Nat. Energy*, 2023, **8**, 159–168.
20 H. Liu, L. Zhao, Y. Ye, X. Yang, Y. Zhang, Q. Li, R. Li, H. Liu, B. Huang and F. Wu, *Chem. Rev.*, 2025, **125**, 9553–9678.
21 Y. Du, S. Deng, Y. Zhu, J. Jiang, G. Yang, M. Wu and Z. Li, *Chem. Soc. Rev.*, 2025, **54**, 8287–8324.
22 Q. He, J. Ning, H. Chen, Z. Jiang, J. Wang, D. Chen, C. Zhao, Z. Liu, I. F. Perepichka and H. Meng, *Chem. Soc. Rev.*, 2024, **53**, 7091–7157.
23 Y. Chen, S. Gao, Y. Su, T. Chen and J. Fu, *Adv. Energy Mater.*, 2025, e02938.
24 C. Zhang, L. Yao, M. Pu and C. Zhou, *RSC Appl. Polym.*, 2025, **3**, 549–573.
25 Y. Zhu, Z. Tang, L. Yuan, B. Li, Z. Shao and W. Guo, *Chem. Soc. Rev.*, 2025, **54**, 1027–1092.
26 D. Meng, M. Xu, S. Li, M. Ganesan, X. Ruan, S. K. Ravi and X. Cui, *Small*, 2024, **20**, 2304483.
27 L. Zhang, R. Feng, W. Wang and G. Yu, *Nat. Rev. Chem.*, 2022, **6**, 524–543.

28 W. Du, X. Du, M. Ma, S. Huang, X. Sun and L. Xiong, *Adv. Funct. Mater.*, 2022, **32**, 2110871.
29 M. Zhang, L. Wang, H. Xu, Y. Song and X. He, *Nano-Micro Lett.*, 2023, **15**, 135.
30 F. Baskoro, A. L. Lubis, H. Q. Wong, G.-S. Liou and H.-J. Yen, *J. Mater. Chem. A*, 2023, **11**, 11210–11221.
31 Z. Song, H. Zhan and Y. Zhou, *Angew. Chem., Int. Ed.*, 2010, **49**, 8444–8448.
32 J. Wang, H. Liu, C. Du, X. Zhang, Y. Liu, H. Yao, Z. Sun and S. Guan, *Chem. Eng. J.*, 2022, **444**, 136598.
33 S. Muench, A. Wild, C. Friebe, B. Häupler, T. Janoschka and U. S. Schubert, *Chem. Rev.*, 2016, **116**, 9438–9484.
34 R. S. Bhatta and M. Tsige, *Polymer*, 2015, **56**, 293–299.
35 T. Lei, J.-Y. Wang and J. Pei, *Acc. Chem. Res.*, 2014, **47**, 1117–1126.
36 J. Xie, P. Gu and Q. Zhang, *ACS Energy Lett.*, 2017, **2**, 1985–1996.
37 T. B. Schon, B. T. McAllister, P.-F. Li and D. S. Seferos, *Chem. Soc. Rev.*, 2016, **45**, 6345–6404.
38 Y. Liang, Z. Tao and J. Chen, *Adv. Energy Mater.*, 2012, **2**, 742–769.
39 H. Lyu, X.-G. Sun and S. Dai, *Adv. Energy Sustainability Res.*, 2021, **2**, 2000044.
40 Z. Song, H. Zhan and Y. Zhou, *Angew. Chem., Int. Ed.*, 2010, **49**, 8444–8448.
41 Y.-T. Chern, C.-C. Yen, J.-M. Wang, I.-S. Lu, B.-W. Huang and S.-H. Hsiao, *Polymers*, 2024, **16**, 1644.
42 D. F. Nugraha, D. Kim, E. Yang, S. W. Lee, D. R. Whang, S. A. Lee, S. H. Park and D. W. Chang, *ACS Appl. Electron. Mater.*, 2023, **5**, 1174–1182.
43 S. Lee, J. E. Kwon, J. Hong, S. Y. Park and K. Kang, *J. Mater. Chem. A*, 2019, **7**, 11438–11443.
44 R. Cheng, X. He, K. Li, B. Ran, X. Zhang, Y. Qin, G. He, H. Li and C. Fu, *Adv. Mater.*, 2024, **36**, 2402184.
45 A. E. Lakraychi, F. Dolhem, A. Vlad and M. Becuwe, *Adv. Energy Mater.*, 2021, **11**, 2101562.
46 X.-H. Chen, H. Lu, Z. Wu, H. Wang, S. Zhang, S. Mei, G. Long, Q. Zhang and C.-J. Yao, *J. Mater. Chem. A*, 2023, **11**, 77–83.
47 Y. Lu, Q. Zhang and J. Chen, *CCS Chem.*, 2023, **5**, 1491–1508.
48 J. Aher, A. Graefenstein, G. Deshmukh, K. Subramani, B. Krueger, M. Haensch, J. Schwenzel, K. Krishnamoorthy and G. Wittstock, *ChemElectroChem*, 2020, **7**, 1160–1165.
49 N. Wang, Y. Wei, S. Yu, W. Zhang, X. Huang, B. Fan, H. Yuan and Y. Tan, *J. Mater. Sci. Technol.*, 2024, **183**, 206–214.
50 Z. Zhao, D. Liu and Y. Wang, *Chem. Commun.*, 2025, **61**, 5842–5856.
51 E. Grignon, A. M. Battaglia, J. T. Liu, B. T. McAllister and D. S. Seferos, *ACS Appl. Mater. Interfaces*, 2023, **15**, 45345–45353.
52 H.-S. Chin, H. Q. Wong, H.-J. Yen and Y.-R. Kung, *ACS Appl. Opt. Mater.*, 2025, **3**, 383–391.
53 K. B. Labasan, H.-J. Lin, F. Baskoro, J. J. H. Togonon, H. Q. Wong, C.-W. Chang, S. D. Arco and H.-J. Yen, *ACS Appl. Mater. Interfaces*, 2021, **13**, 17467–17477.
54 J. Wang, H. Yao, C. Du and S. Guan, *J. Power Sources*, 2021, **482**, 228931.
55 F. Baskoro, P.-C. Chiang, Y.-C. Lu, J. N. Patricio, S. D. Arco, H.-C. Chen, W.-S. Kuo, L.-L. Lai and H.-J. Yen, *Electrochim. Acta*, 2022, **434**, 141306.
56 E. Peled and S. Menkin, *J. Electrochem. Soc.*, 2017, **164**, A1703.
57 S. Lee, G. Kwon, K. Ku, K. Yoon, S. K. Jung, H. D. Lim and K. Kang, *Adv. Mater.*, 2018, **30**, 1704682.
58 S. Renault, V. A. Oltean, C. M. Araujo, A. Grigoriev, K. Edström and D. Brandell, *Chem. Mater.*, 2016, **28**, 1920–1926.
59 H. Yang, S. Liu, L. Cao, S. Jiang and H. Hou, *J. Mater. Chem. A*, 2018, **6**, 21216–21224.
60 X. Han, G. Qing, J. Sun and T. Sun, *Angew. Chem.*, 2012, **124**, 5237–5241.
61 Z. Man, P. Li, D. Zhou, R. Zang, S. Wang, P. Li, S. Liu, X. Li, Y. Wu and X. Liang, *J. Mater. Chem. A*, 2019, **7**, 2368–2375.
62 H. Kang, H. Liu, C. Li, L. Sun, C. Zhang, H. Gao, J. Yin, B. Yang, Y. You and K.-C. Jiang, *ACS Appl. Mater. Interfaces*, 2018, **10**, 37023–37030.
63 J. Li, M. Luo, Z. Ba, Z. Wang, L. Chen, Y. Li, M. Li, H.-B. Li, J. Dong and X. Zhao, *J. Mater. Chem. A*, 2019, **7**, 19112–19119.
64 F. Baskoro, C.-M. Ngue, K. B. Labasan, H. Q. Wong, M.-K. Leung and H.-J. Yen, *Energy Technol.*, 2021, **9**, 2100212.
65 J. S. Ko, V. V. Doan-Nguyen, H.-S. Kim, G. A. Muller, A. C. Serino, P. S. Weiss and B. S. Dunn, *ACS Appl. Mater. Interfaces*, 2017, **9**, 1416–1425.
66 J. Wang, J. Polleux, J. Lim and B. Dunn, *J. Phys. Chem. C*, 2007, **111**, 14925–14931.
67 Y. Gogotsi and P. Simon, *Science*, 2011, **334**, 917–918.
68 V. Augustyn, P. Simon and B. Dunn, *Energy Environ. Sci.*, 2014, **7**, 1597–1614.
69 P. Taberna, P. Simon and J.-F. Fauvarque, *J. Electrochem. Soc.*, 2003, **150**, A292.

